

# Interfacial Micellar Structures from Novel Amphiphilic Star Polymers

Kirsten L. Genson,<sup>†</sup> Joshua Hoffman,<sup>†</sup> Jing Teng,<sup>†</sup> Eugene R. Zubarev,<sup>†</sup>  
David Vaknin,<sup>‡</sup> and Vladimir V. Tsukruk<sup>\*,†</sup>

Department of Materials Science and Engineering, Iowa State University, Ames, Iowa 50011,  
and Ames Laboratory and Department of Physics and Astronomy, Iowa State University,  
Ames, Iowa 50011

Received June 11, 2004. In Final Form: August 4, 2004

An amphiphilic heteroarm star polymer containing 12 alternating hydrophobic/hydrophilic arms of polystyrene (PS) and poly(acrylic acid) (PAA) connected to a well-defined rigid aromatic core was studied at the air–water and the air–solid interfaces. At the air–water interface, the molecules spontaneously form pancakelike micellar aggregates which measure up to several microns in diameter and 5 nm in thickness. Upon reduction of the surface area per molecule to 7 nm<sup>2</sup>, the two-dimensional micelles merged into a dense monolayer. We suggest that confined phase separation of dissimilar polymer arms occurred upon their segregation on the opposite sides of the rigid disklike aromatic core, forcing the rigid cores to adopt a face-on orientation with respect to the interface. Upon transfer onto solid supports the PS chains face the air–film interface making it completely hydrophobic, and the PAA chains were found to collapse and form a thin flattened underlayer. This study points toward new strategies to create large 2D microstructures with facial amphiphilicity and suggests a profound influence of star molecular architecture on the self-assembly of amphiphiles at the air–water interface.

## Introduction

Star block copolymers possess an unusual molecular architecture which often generates properties not observed in linear analogues.<sup>1,2</sup> The self-assembling behavior of amphiphilic star polymers in selective solvents is particularly interesting. To this end, spherical,<sup>3</sup> cylindrical,<sup>4</sup> and vesicular<sup>5</sup> micelles have recently been documented by several research groups. By way of contrast, little is known about their behavior at the air–water interface and how it compares to linear diblock systems which were studied for several systems. Examples of the interfacial structures of homopolymers<sup>6</sup> and amphiphilic block co-

polymers were previously described.<sup>7</sup> Eisenberg and co-workers<sup>7</sup> reported on the discovery of surface micelles of polystyrene–poly(4-vinylpyridine) which formed spontaneously at the air–water interface. Such structures were fairly uniform and consisted of ~100 individual molecules. Another example of an amphiphile studied directly at the air–water interface was polystyrene (PS)–poly(ethylene oxide) (PEO) as described by Silva et al.<sup>8</sup> and Lennox et al.<sup>9</sup> It was shown that this copolymer forms highly ordered 2D arrays of spherical micelles at moderate surface pressure, although the actual mechanism of their formation remains highly debatable. Interestingly, several nonamphiphilic block copolymers such as PS/poly(*tert*-butyl methacrylate), PS/poly(*tert*-butyl acrylate), PS/poly(*n*-butyl methacrylate), and PS/poly(dimethylsiloxane) behave at the air–water interface in a manner similar to that of amphiphiles, which appears to be a universal behavior of diblock copolymers mainly defined by the volume ratio of the incompatible blocks.<sup>10</sup> A number of linear PS–poly(acrylic acid) (PAA) block copolymers have been studied in selective solvents, solid surfaces, and air–water interfaces, and a variety of micellar structures and aggregates have been observed with shape, size, and

<sup>†</sup> Department of Materials Science and Engineering.

<sup>‡</sup> Ames Laboratory and Department of Physics and Astronomy.

\* To whom correspondence should be addressed: e-mail vladimir@iastate.edu.

(1) (a) Hadjichristidis, N.; Pitsikalis, M.; Pispas, S.; Iatrou, H. *Chem. Rev.* **2001**, *101*, 3747. (b) Hong, K.; Uhrig, D.; Mays, J. W. *Curr. Opin. Solid State Mater. Sci.* **1999**, *4*, 531. (c) Coessens, V.; Pintauer, T.; Matyjaszewski, K. *Prog. Polym. Sci.* **2001**, *26*, 337. (d) Hawker, C. J.; Bosman, A. W.; Harth, E. *Chem. Rev.* **2001**, *101*, 3661.

(2) (a) Jacob, S.; Majoros, I.; Kennedy, J. P. *Macromolecules* **1996**, *29*, 8631. (b) Heise, A.; Hedrick, J. L.; Frank, C. W.; Miller, R. D. *J. Am. Chem. Soc.* **1999**, *121*, 8647. (c) Heise, A.; Trollsas, M.; Magbitang, T.; Hedrick, J. L.; Frank, C. W.; Miller, R. D. *Macromolecules* **2001**, *34*, 2798. (d) Ohno, K.; Wong, B.; Haddleton, D. M. *J. Polym. Sci., Polym. Chem.* **2001**, *39*, 2206. (e) Angot, S.; Murthy, K. S.; Taton, D.; Gnanou, Y. *Macromolecules* **1998**, *31*, 7218. (f) Ueda, J.; Kamigaito, M.; Sawamoto, M. *Macromolecules* **1998**, *31*, 6762. (g) Klok, H. A.; Hernandez, J. R.; Becker, S.; Mullen, K. J. *J. Polym. Sci., Polym. Chem.* **2001**, *39*, 1572. (h) Hirao, A.; Hayashi, M.; Tokuda, Y.; Haraguchi, N.; Higashihara, T.; Ryu, S. W. *Polym. J.* **2002**, *34*, 633. (i) Hou, S.; Chaikof, E. L.; Taton, D.; Gnanou, Y. *Macromolecules* **2003**, *36*, 3874. (j) Francis, R.; Taton, D.; Logan, J. L.; Masse, P.; Gnanou, Y.; Duran, R. S. *Macromolecules* **2003**, *36*, 8253.

(3) (a) Voulgaris, D.; Tsitsilianis, C.; Esselink, F. J.; Hadziioannou, G. *Polymer* **1998**, *39*, 6429. (b) Voulgaris, D.; Tsitsilianis, C.; Grayer, V.; Esselink, F. J.; Hadziioannou, G. *Polymer* **1999**, *40*, 5879. (c) Tsitsilianis, C.; Voulgaris, D.; Stepanek, M.; Podhajecka, K.; Prochazka, K.; Tuzar, Z.; Brown, W. *Langmuir* **2000**, *16*, 6868. (d) Voulgaris, D.; Tsitsilianis, C. *Macromol. Chem. Phys.* **2001**, *202*, 3284.

(4) Teng, J.; Zubarev, E. R. *J. Am. Chem. Soc.* **2003**, *125*, 11840.

(5) Jin, R. H. *Macromol. Chem. Phys.* **2003**, *204*, 403.

(6) (a) Granick, S. *Macromolecules* **1985**, *18*, 1597. (b) Kawaguchi, M.; Sauer, B. B.; Yu, H. *Macromolecules* **1989**, *22*, 1735. (c) Brinkhuis, R. H. G.; Schouthern, M. J. *Macromolecules* **1991**, *24*, 1487.

(7) (a) Zhu, J.; Eisenberg, A.; Lennox, R. B. *J. Am. Chem. Soc.* **1991**, *113*, 5583. (b) Zhu, J.; Lennox, R. B.; Eisenberg, A. *Langmuir* **1991**, *7*, 11579. (c) Zhu, J.; Eisenberg, A.; Lennox, R. B. *Makromol. Chem.* **1992**, *53*, 211. (d) Zhu, J.; Lennox, R. B.; Eisenberg, A. *J. Phys. Chem.* **1992**, *96*, 4727. (e) Zhu, J.; Eisenberg, A.; Lennox, R. B. *Macromolecules* **1992**, *25*, 6547. (f) Zhu, J.; Eisenberg, A.; Lennox, R. B. *Macromolecules* **1992**, *25*, 6556.

(8) (a) Gonçalves da Silva, A. M.; Filipe, E. J. M.; d'Oliveira, J. M. R.; Martinho, J. M. G. *Langmuir* **1996**, *12*, 6547. (b) Gonçalves da Silva, A. M.; Simoes Gamboa, A. L.; Martinho, J. M. G. *Langmuir* **1998**, *14*, 5327.

(9) Cox, J. K.; Yu, K.; Constantue, B.; Eisenberg, A.; Lennox, R. B. *Langmuir* **1999**, *15*, 7714.

(10) Li, S.; Hanley, S.; Khau, I.; Varshney, S. K.; Eisenberg, A.; Lennox, R. B. *Langmuir* **1993**, *9*, 2243.

symmetry depending upon their chemical composition and molecular weight.<sup>11,12</sup>

Very recently, Gnanou and Duran<sup>13</sup> described interfacial structures of core-shell PS-PEO star amphiphile with three diblock arms deposited on a solid surface. Spherical micellar structures imaged by atomic force microscopy (AFM) on solid substrates were very similar to those observed in linear analogues because, probably, each PEO block in that core-shell structure had two junction points connecting it to the core and the peripheral PS block. In general, this intrinsic feature of core-shell star amphiphiles imposes a significant limitation on the ability of incompatible arms to rearrange in response to selective environment. An excellent alternative in that respect is offered by heteroarm stars where both types of arms are directly linked to the core and therefore have only one junction point.

Because of synthetic challenges, the heteroarm amphiphilic stars with alternating dissimilar arms are not readily available, and only few examples have been described to date with main attention paid to the bulk structure and phase behavior of these polymers and surface films cast from solution.<sup>14</sup> AFM studies of single molecules of PS-P2VP star polymers demonstrated the heteroarm star polymer showed a pronounced segregation of the polymer arms in selective solvent conditions, and the inclusion of metal clusters among the polymer arms allowed for direct calculation of the number of arms per core. The PS-PAA heteroarm amphiphile with a well-defined rigid core was recently reported by Zubarev et al.,<sup>4</sup> who observed rich self-assembling properties in selective solvents. Both spherical and cylindrical supermicelles were found in water and methanol as well as reverse supermicelles in nonpolar organic media. However, the question of the interfacial behavior of this amphiphilic star polymer with shape-persistent core remains open.

Here we report our studies on the interfacial behavior of this star block copolymer containing 12 alternating arms of PAA and PS attached to a rigid aromatic core (Figure 1).<sup>4</sup> The number of monomeric units was  $m = n = 25$  for symmetric star block copolymer and  $m = 30$  and  $n = 40$  for asymmetric star amphiphile. We examine the structures formed at the air-water and the air-solid interfaces in attempt to reveal the influence of molecular architecture and the volume fraction of different blocks on the self-organization process at air-water interface and solid surface in comparison with regular linear PS-PAA block copolymers.

## Experimental Section

The synthesis, chemical composition, and solution properties of heteroarm star amphiphiles (PAA<sub>25</sub>)<sub>6</sub>-s-(PS<sub>25</sub>)<sub>6</sub> and (PAA<sub>30</sub>)<sub>6</sub>-s-(PS<sub>40</sub>)<sub>6</sub> have been described in detail elsewhere.<sup>4</sup> Monomolecular films of the star polymer were prepared by the Langmuir technique on an RK-1 trough (Riegel & Kirstein, GmbH) according

(11) Zhang, W.; Shi, L.; An, Y.; Shen, X.; Guo, Y.; Gao, L.; Liu, Z.; He, B. *Langmuir* **2003**, *19*, 6026.

(12) (a) Zhang, L.; Eisenberg, A. *Science* **1995**, *268*, 1728. (b) Li, S.; Clarke, C. J.; Lennox, R. B.; Eisenberg, A. *Colloids Surf. A* **1998**, *133*, 191. (c) Terreau, O.; Luo, L.; Eisenberg, A. *Langmuir* **2003**, *19*, 5601. (d) Li, S.; Clarke, C. J.; Eisenberg, A.; Lennox, R. B. *Thin Solid Films* **1999**, *354*, 136. (e) Schmitter, M.; Engelking, J.; Heise, A.; Miller, R. B.; Menzel, H. *Macromol. Chem. Phys.* **2000**, *201*, 1504.

(13) Francis, R.; Skolnik, A. M.; Carino, S. A. R.; Logan, J. L.; Underhill, R. S.; Angot, S.; Taton, D.; Gnanou, Y.; Duran, R. S. *Macromolecules* **2002**, *35*, 6483.

(14) (a) Kiriy, A.; Gorodyska, G.; Minko, S.; Tsitsilianis, C.; Jaeger, W.; Stamm, M. *J. Am. Chem. Soc.* **2003**, *125*, 11202. (b) Gorodyska, G.; Kiriy, A.; Minko, S.; Tsitsilianis, C.; Stamm, M. *Nano Lett.* **2003**, *3*, 365. (c) Kiriy, A.; Gorodyska, G.; Minko, S.; Stamm, M.; Tsitsilianis, C. *Macromolecules* **2003**, *36*, 8704.

to the usual procedure adapted in our lab.<sup>15</sup> The trough was placed in a laminar flow hood. The compounds were dissolved in chloroform (Fisher, reagent grade) to ~0.01 mmol/L concentration. The solution was spread over the water (NanoPure, > 18 MΩ cm) subphase and dried for 30 min before compression. Monomolecular films were deposited using the Langmuir-Blodgett (LB) technique on cleaned silicon substrates (Semiconductor Processing Co.). Silicon wafers were treated in "piranha" solution (30% hydrogen peroxide:94% sulfuric acid, 1:3, *chemical hazard!*) according to the standard procedure.<sup>16</sup>

Ellipsometric measurements of monolayer thickness were carried out with a COMPEL automatic ellipsometer (InOmTech, Inc.). Contact angle measurements were performed with the sessile droplet method. Imaging of the monolayers was performed with AFM microscopes, Dimension-3000 and Multimode (Digital Instruments), in the light tapping mode according to an experimental procedure described elsewhere.<sup>17-19</sup> Surfaces of LB monolayer were probed at several random locations with widely varying scan sizes from 0.3 to 30 μm. The geometrical parameters of all molecules were estimated from molecular models built with the Materials Studio 3.0 software package and the Cerius<sup>2</sup> program on a SGI workstation. The combination of molecular dynamics and energy minimization was used to generate molecular models.

X-ray reflectivity measurements of the Langmuir monolayers directly at the air-water interface were conducted on the liquid-surface X-ray spectrometer at the 6ID beamline at the Advanced Photon Source synchrotron at Argonne National Laboratory according to the usual procedure adapted in our lab and described in the literature.<sup>20-22</sup> Monomolecular films were prepared by the Langmuir technique on a temperature-controlled, Teflon trough sealed within a helium filled chamber to reduce the background scattering from air and reduce oxidation reaction that can damage the monolayer. A downstream silicon double-crystal monochromator was used to select the X-ray beam at the desired energy ( $\lambda = 0.0776$  nm).

## Results and Discussion

**Surface Behavior.** Both heteroarm star block copolymers studied here possess well-defined star shape with dissimilar arms attached to the rigid, shape persistent core as visualized by molecular models presented in Figure 1. In an extended conformation and face-on orientation, the molecules occupy very large surface areas with the diameter of 17 and 24 nm for (PAA<sub>25</sub>)<sub>6</sub>-s-(PS<sub>25</sub>)<sub>6</sub> and (PAA<sub>30</sub>)<sub>6</sub>-s-(PS<sub>40</sub>)<sub>6</sub> molecules, respectively (Table 1). In this conformation, the rigid core occupies a small surface area as compared to polymer arms, and significant free surface is available between adjacent arms.

These molecules formed stable Langmuir monolayers at the air-water interface and showed the classical pressure vs molecular area ( $\pi$ -A) behavior without any significant plateau at intermediate pressures (Figure 2).

(15) (a) Peleshanko, S.; Sidorenko, A.; Larson, K.; Villavicencio, O.; Ornatska, M.; McGrath, D. V.; Tsukruk, V. V. *Thin Solid Films* **2002**, *406*, 233. (b) Sidorenko, A.; Houphouet-Boigny, C.; Villavicencio, O.; McGrath, D. V.; Tsukruk, V. V. *Thin Solid Films* **2002**, *410*, 147.

(16) (a) Tsukruk, V. V. *Adv. Mater.* **2001**, *13*, 95. (b) Tsukruk, V. V.; Bliznyuk, V. N.; Hazel, J.; Visser, D.; Everson, M. P. *Langmuir* **1996**, *12*, 4840. (c) Bliznyuk, V. N.; Everson, M. P.; Tsukruk, V. V. *J. Tribol.* **1998**, *120*, 489.

(17) Tsukruk, V. V. *Rubber Chem. Technol.* **1997**, *70*, 430.

(18) Tsukruk, V. V.; Reneker, D. H. *Polymer* **1995**, *36*, 1791.

(19) Ratner, B.; Tsukruk, V. V., Eds.; *Scanning Probe Microscopy of Polymers*; ACS Symp. Ser. **1998**, *694*.

(20) (a) Vaknin, D. In *Methods of Materials Research*; Kaufmann, E. N.; Abbaschian, R.; Baines, P. A.; Bocarsly, A. B.; Chien, C. L.; Doyle, B. L.; Fultz, B.; Leibowitz, L.; Mason, T.; Sanches, J. M., Eds.; John Wiley & Sons: New York, 2001; p 10d.2.1. (b) Vaknin, D.; Kelley, M. S. *Biophys. J.* **2000**, *79*, 2616.

(21) Weissbuch, I.; Leveiller, F.; Jacquemain, D.; Kjaer, K.; Al-Nielsen, J.; Leiserowitz, L. *J. Phys. Chem.* **1993**, *97*, 12858.

(22) (a) Larson, K.; Vaknin, D.; Villavicencio, O.; McGrath, D. V.; Tsukruk, V. V. *J. Phys. Chem. B* **2002**, *106*, 7246. (b) Genson, K. L.; Vaknin, D.; Villavicencio, O.; McGrath, D. V.; Tsukruk, V. V. *J. Phys. Chem. B* **2002**, *106*, 11277.

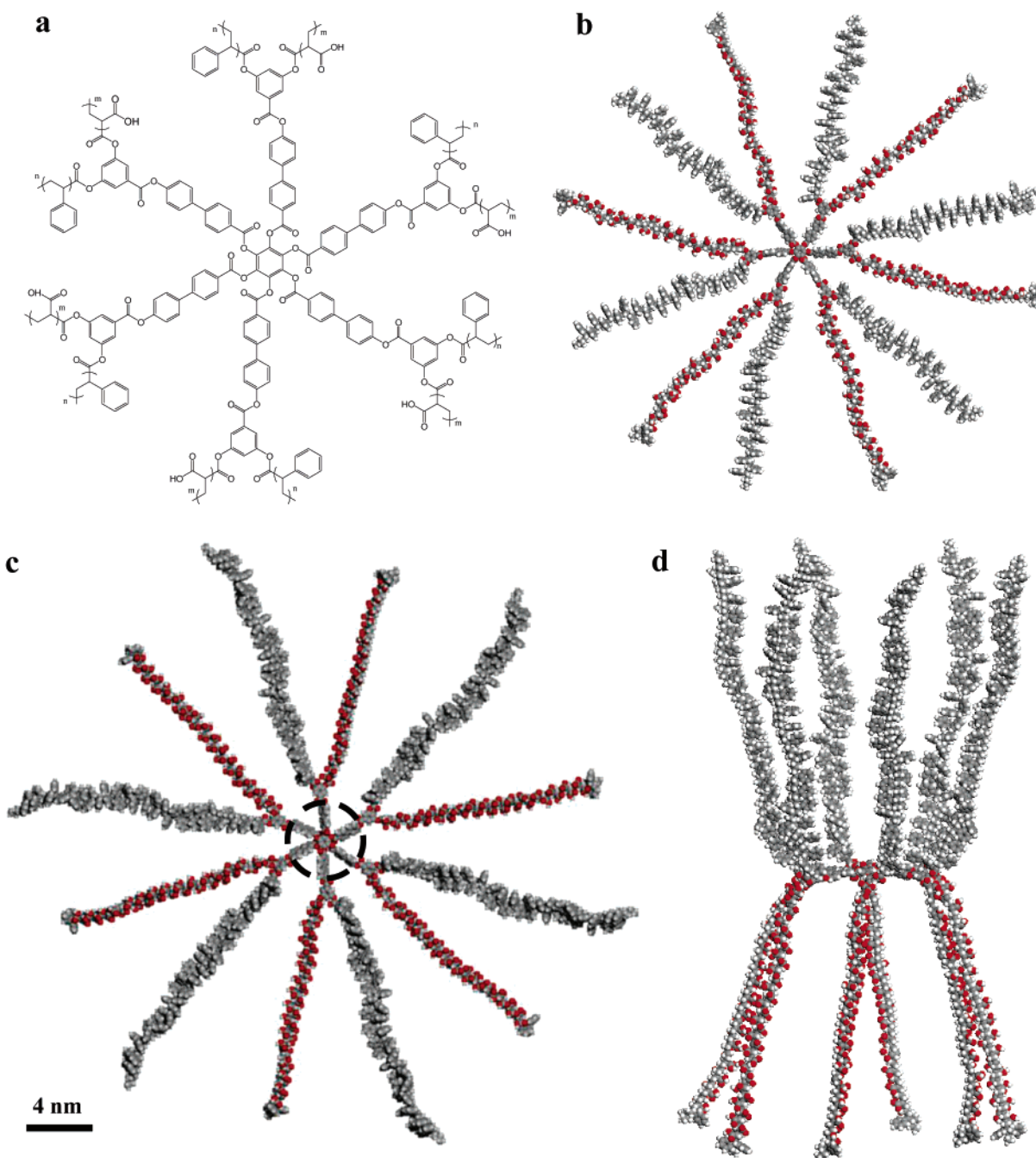


**Figure 1.** (a) Chemical formula of  $(\text{PAA}_m)_6\text{-s-(PS}_n)_6$ , (b) molecular model of  $(\text{PAA}_{25})_6\text{-s-(PS}_{25})_6$ , (c) molecular model of  $(\text{PAA}_{30})_6\text{-s-(PS}_{40})_6$ , and (d) side view of  $(\text{PAA}_{30})_6\text{-s-(PS}_{40})_6$  with a spatial separation of hydrophobic PS and hydrophilic PAA arms placed above and below the aromatic core, respectively. Dashed circle represents the calculated core area.

This shape of the isotherms indicated an absence of any significant structural rearrangements within compressed monolayer usually observed for amphiphilic block copolymers with comparable composition (content of hydrophilic block of about 30%, Table 1). Detectable increase in the surface pressure was observed for the surface area per molecule below  $20 \text{ nm}^2$  that is much smaller than the surface area per molecule estimated for extended conformation and face-on orientation (Figure 1). This indicates significant overlap of the molecules upon compression or reorganization of their conformation under very low pressures.

The steady growth of pressure as the cross-sectional area decreased with the limiting value for  $(\text{PAA}_{25})_6\text{-s-(PS}_{25})_6$  star slightly lower ( $9 \text{ nm}^2$ ) than that for  $(\text{PAA}_{30})_6\text{-s-(PS}_{40})_6$

star ( $10 \text{ nm}^2$ ) (Figure 2). These values are close to the cross-sectional area of the rigid core region (shown in Figure 1 as dashed circle) calculated to be  $9.6 \text{ nm}^2$  (excluding the space between adjacent arms) for either 12-arm star polymer. The very modest increase in cross-sectional area for the larger asymmetric star molecules and very similar shape of the isotherms indicated the molecular packing is only slightly affected by the bulkier PS chains. On the other hand, both values are close to the core area, indicating that dense lateral packing of rigid cores is a defining factor in the formation of condensed monolayer with both types of arms playing a minor role at highest packing densities (Figure 1).

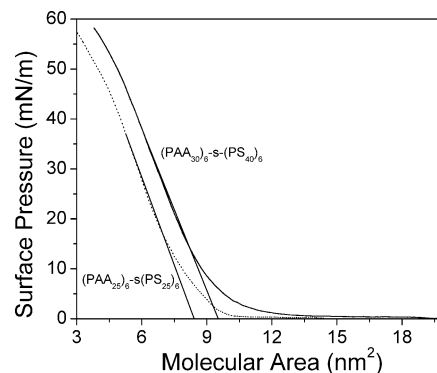
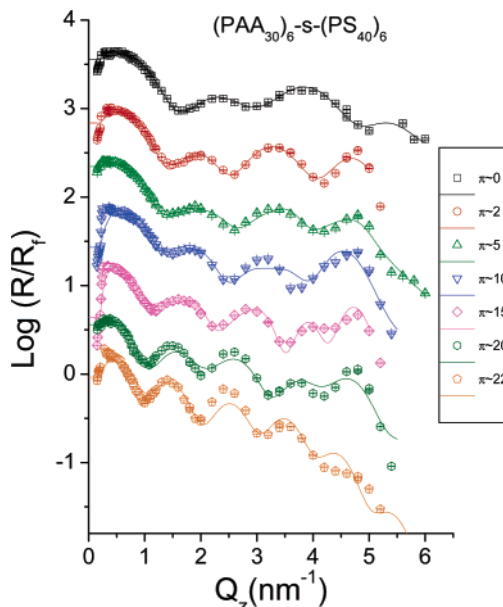
This interfacial behavior under compression suggests that the PAA and PS arms are disassociated from the

**Table 1. Molecular Dimensions of the 12-Arm Star Polymers**

	(PAA <sub>30</sub> ) <sub>6</sub> -s-(PS <sub>40</sub> ) <sub>6</sub>	(PAA <sub>25</sub> ) <sub>6</sub> -s-(PS <sub>25</sub> ) <sub>6</sub>
core diameter (nm)	4.2	4.2
total diameter (nm)	23.9	17.4
PS extended length (nm)	10.0	6.6
PAA extended length (nm)	8.7	6.8
PS end-to-end distance (nm)	2.3	2.0
PAA end-to-end distance (nm)	1.9	1.8
area of core (nm <sup>2</sup> )	9.6	9.6
A <sub>0</sub> (nm <sup>2</sup> )	10.0	9.1
area of coiled PS arm (nm <sup>2</sup> )	2.2	1.6
area of coiled PAA arm (nm <sup>2</sup> )	1.6	1.3
volume of PS arm (nm <sup>3</sup> )	6.5	4.1
volume of PAA arm (nm <sup>3</sup> )	3.1	2.6
PAA volume fraction	0.29	0.35

plane of the core upon compression to the condensed state (see a simple model with oppositely extended arms in Figure 1). It is clear that actual state of the arms is different from this simple molecular graphics representation and should include different levels of ordering. Considering this surface behavior and the architecture of the star molecule and literature data, it is reasonable to expect that hydrophilic PAA arms were submerged into the water subphase whereas the hydrophobic PS arms are packed above the air–water interface, effectively pinning the core plane. The calculated cross-sectional area on the larger PS arms in coiled state was 2.17 nm<sup>2</sup> per arm while the shorter PS arms should occupy 1.63 nm<sup>2</sup> (Table 1). Taking into account the six PS arms attached to each aromatic core, the cross-sectional area per molecule with coiled arms for (PAA<sub>30</sub>)<sub>6</sub>-s-(PS<sub>40</sub>)<sub>6</sub> was estimated as 13.1 nm<sup>2</sup> and 9.8 nm<sup>2</sup> for (PAA<sub>25</sub>)<sub>6</sub>-s-(PS<sub>25</sub>)<sub>6</sub>, which is close but still below the onset of formation of the condensed monolayer.

The decrease in cross-sectional area below these values should force the flexible arms to elongate in the vertical direction, thereby decreasing the effective cross-sectional area per molecule. However, we suggest that the transformation to truly brushlike packing regime is not possible in this system due to the presence of rigid disklike core, limiting effective grafting density of flexible chains to 1.6 nm<sup>2</sup>/chain. It is important to emphasize that arms are not emanating from one and the same point as usually happens in conventional star polymers but rather from six equidistant peripheral points of a fairly large and rigid core (4.2 nm) that keeps the junction points of arms spatially separated. In addition, considering that the PS block at room temperature is well below the glass transition (even accounting for low molecular weight and possible presence of trapped residual solvent) and the mobility and compressibility of the PS phase will be severely limited, it is safe to suggest that the state of PS blocks will stay virtually unchanged. As a result, even at high pressure the PS arms will stay in a collapsed state covering the aromatic core. The same limitation is imposed by the core on the hydrophilic PAA arms submerged in the water subphase, but because of their dissolved state they remain mobile enough to change their state (to that allowed by the limiting grafting density) under compression. We suggest that this key difference between the star-shaped molecules with sizable rigid core and diblock amphiphiles that do not have the incompressible core and therefore can undergo the pancake–brush transformation at high surface pressures defines the shape of the Langmuir isotherms observed here. To corroborate this hypothesis and to obtain insights into the structure of the monolayers, we used X-ray reflectivity measurements and AFM imaging as discussed below.

**Figure 2.**  $\pi$ - $A$  isotherm of (PAA<sub>30</sub>)<sub>6</sub>-s-(PS<sub>40</sub>)<sub>6</sub> (solid line) and (PAA<sub>25</sub>)<sub>6</sub>-s-(PS<sub>25</sub>)<sub>6</sub> (dashed line).**Figure 3.** X-ray reflectivity data and model for (PAA<sub>30</sub>)<sub>6</sub>-s-(PS<sub>40</sub>)<sub>6</sub> at different surface pressures. Data represented by symbols and model represented by line. Intensities offset for clarity.

**Interfacial Organization of Langmuir Monolayers.** Because the data for star molecule with shorter arms were not sufficient quality, we will concentrate here on (PAA<sub>30</sub>)<sub>6</sub>-s-(PS<sub>40</sub>)<sub>6</sub> molecules. The X-ray reflectivity curves for this molecule displayed multiple minima at all surface pressures (Figure 3). X-ray reflectivity measurement for the larger 12-arm star polymer before compression showed three well-defined minima, signifying an organized monolayer formation. At higher surface pressure, the minima became more defined and the spacing decreased, indicating an increase in monolayer thickness and the chain elongation (Figure 3). The overall angular variation of intensity decreased much faster at higher pressures which suggested the sharpening of the monolayer interfaces. These results demonstrate that the (PAA<sub>30</sub>)<sub>6</sub>-s-(PS<sub>40</sub>)<sub>6</sub> molecules formed dense uniform monolayers at all pressures with the overall thickness increasing as the surface pressure is raised.

The reflectivity data were modeled using a four-box model as presented in Figure 4 along with examples of spread and compressed molecules built with consideration of most critical parameters (overall thickness, separate thicknesses of PS and PAA phases, and cross-sectional area per molecule) (Table 2). These boxes with constant electron density represented the submerged PAA chains, the core region, the mixed collapsed, and the extended PS

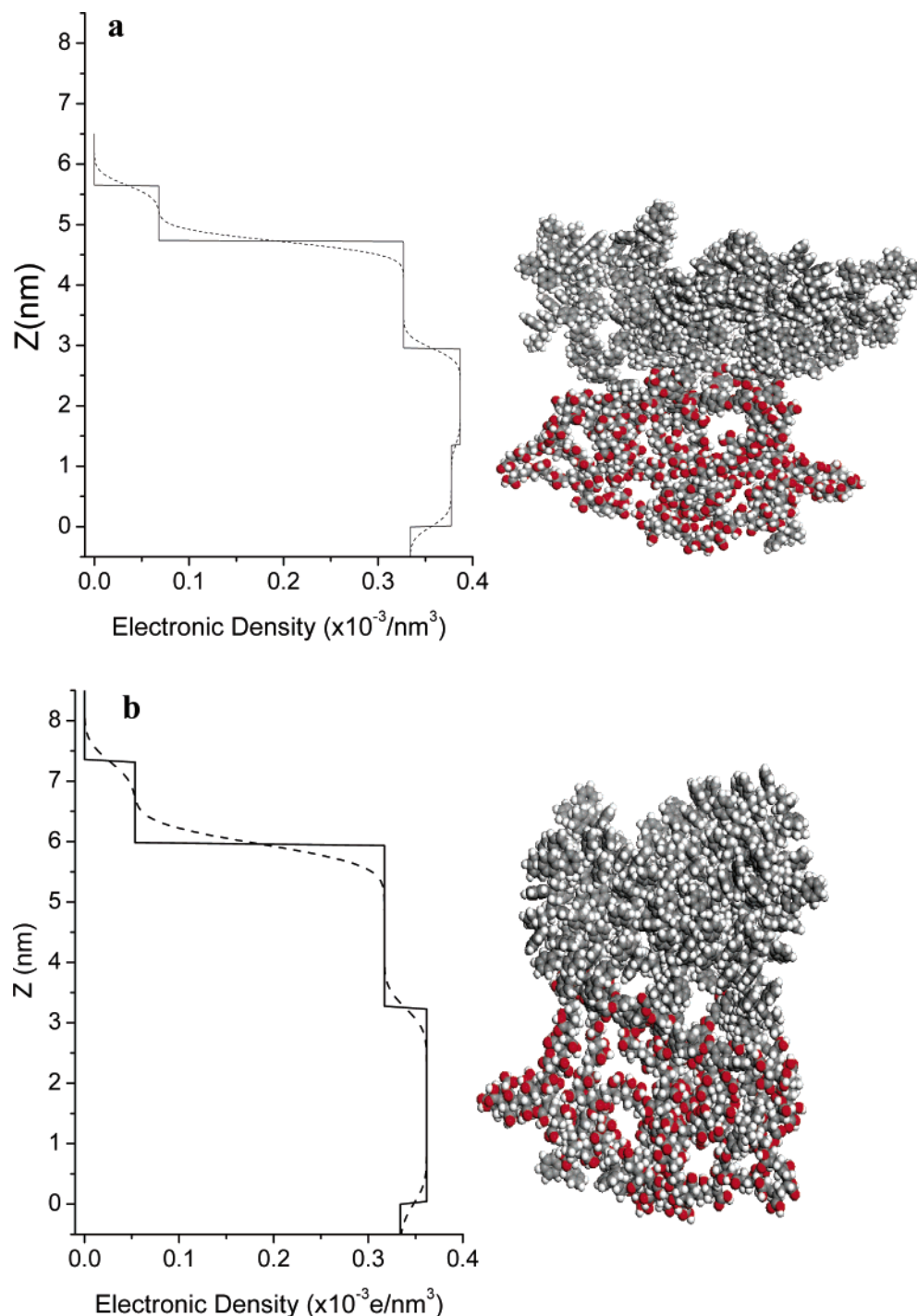


**Figure 4.** Box models of  $(\text{PAA}_{30})_6\text{-s-(PS}_{40})_6$  at (a) low-pressure regime (2 mN/m) and (b) high-pressure regime (20 mN/m). Corresponding molecular models shown to the right.

chains.<sup>23</sup> At low surface pressure and large cross-sectional area electron density distribution confirmed a clearly organized monolayer with defined layered structure. The slight difference in electronic density at the water surface for the first two blocks ( $0.365 \times 10^3$  and  $0.368 \times 10^3 \text{ e}/\text{nm}^3$ , respectively) corresponding to PAA arms and the aromatic core indicated a slight shift in density of the polymeric chains. The confinement of the hydrophobic aromatic core within a plane created a densely packed layer above the hydrophilic PAA chains. Considering the thickness of the first box of 1.25 nm close to the PAA chain dimensions

(Tables 1 and 2), we can suggest that the hydrated PAA chains are randomly coiled underneath the aromatic core (Figure 4a). The densest region of the film was located near the air–water interface associated with the aromatic cores (second box, Table 2). The PS chains (third box) formed a dense layer of 1.7 nm thick above the water surface, which is close to but slightly lower than the PS random coil size and indicates the collapsed state of the PS chains with density close to but slightly below that for the bulk PS. The presence of the fourth box with extremely low electron density ( $0.048 \times 10^3 \text{ e}/\text{nm}^3$ ) indicated the extension of some PS chains beyond the collapsed PS layer (Figure 4a).

(23) Gregory, B. W.; Vaknin, D.; Gray, J. D.; Ocko, B. M.; Stroeve, P.; Cotton, T. M.; Struve, W. S. *J. Phys. Chem. B* **1997**, *101*, 2006.

**Table 2.** Comparison of Box Model Parameters of PAA<sub>6</sub>-b-PS<sub>6</sub> Star Polymer

box model parameters		surface pressure (mN/m)				
		0	2	10	20	22
first box	length (nm)	1.25	1.36	2.77	3.24	6.25
	electronic density ( $\times 10^3$ e/nm <sup>3</sup> )	0.365	0.377	0.376	0.362	0.386
second box	length (nm)	1.05	1.60	1.77		
	electronic density ( $\times 10^3$ e/nm <sup>3</sup> )	0.368	0.387	0.575		
third box	length (nm)	1.75	1.76	1.48	2.72	
	electronic density ( $\times 10^3$ e/nm <sup>3</sup> )	0.315	0.327	0.331	0.317	
fourth box	length (nm)	1.11	0.934	1.65	1.37	1.55
	electronic density ( $\times 10^3$ e/nm <sup>3</sup> )	0.048	0.068	0.108	0.053	0.05
surface roughness (nm)		0.20	0.173	0.264	0.281	0.28
total thickness (nm)		5.16	5.65	7.67	7.33	7.8
PS thickness (nm)		2.86	2.69	3.13	3.18	3.09

Upon compressing the monolayer to the low pressure regime (from 0 to 2 mN/m), the four-box model showed an overall increase in length and electronic density for all boxes, indicating the monolayer became more densely packed as the chains elongated. The overall thickness increased from 5.2 nm for the monolayer before compression to 5.7 nm at higher pressure of 2 mN/m (Table 2). The cross-sectional area decrease forces the chains to elongate slightly in the vertical direction to compensate for the overall decrease in area. More significant, all four boxes increased in electronic density with a clearer distinction between the first two boxes. These two boxes containing the PAA chains became slightly denser although the boxes lengthened moderately (from 1.05 to 1.60 nm for the second box) while the third and fourth boxes containing the PS chains remained with similar thickness while increasing in density.

The overall thickness of the Langmuir monolayer as well as the density increased for all layers as the surface pressure increased from 2 to <20 mN/m as was indicated above (Figure 3, Table 2). At the intermediate pressures, the monolayer was modeled using four box models with the steadily increased thickness and electronic density for the first box from 1.3 to 2.8 nm, indicating the significant *extension of PAA chains* submerged in the water subphase (Figure 4b). The thickness exceeds the PAA chain dimensions pointing out on initial elongation of the submerged PAA chains. The second box associated mainly with the aromatic cores remained the densest region of the layer. The third box associated with the PS chains very modestly increased in thickness.

For the highest surface pressures corresponding to the condensed state of the monolayer ( $\geq 20$  mN/m), two- and three-box models were used to analyze the data. Although fitting of experimental data for complex multilayered structures is always a challenge, the presence of several well-defined minima and comparison with expected molecular dimensions and electron densities make the results obtained very unambiguous. The first box was assigned to the submerged PAA chains, and the second and third boxes were assigned to the collapsed and extended PS arms, respectively (Figure 4b). The lack of resolution and small difference in electronic densities at higher surface pressures did not allow the aromatic core region to be distinguished from the hydrated and densely packed PAA chains for the highest pressure studied here. The higher electronic density of the first box inferred the molecular core was located in the PAA box increasing the effective density (Table 2). Unlike the lower surface pressures where a dense region contained the aromatic core and parts of the PAA and PS chains, the model for the 20 mN/m monolayer demonstrated a clearly defined transition between the PAA and PS chains. The lower electronic density of the second box ( $0.317 \times 10^3$  e/nm<sup>3</sup>) confirmed the presence of collapsed PS arms located above the air-

water interface, thereby pinning the aromatic core at the interface. Upon reaching the highest surface pressure the vertical electron density distribution can be described the best with a two-box model with the insignificant difference in density between the PAA and PS phases, except some very low-density region on a top of the layer indicating, probably, initial stage of the monolayer collapse. The total thickness of the monolayer increased to 7.9 nm at the highest surface pressure (Table 2). Considering that the density of packing of PAA and PS became indistinguishable, we cannot estimate separate PS and PAA layer thicknesses in this state.

**Monolayer Organization at Solid Surfaces.** AFM imaging of LB monolayers deposited on a hydrophilic silicon surface provided additional information about morphology of monolayers, assuming that the monolayer morphology was not altered by the monolayer transfer that was usually suggested for organic monolayers.<sup>24,25</sup> As was observed, at very low compression (large surface area per molecule) the molecules already formed initial micellar morphology. The monolayer deposited at 20 nm<sup>2</sup> per molecule (twice the limiting cross-sectional area) showed large circular domains of various sizes packed loosely with limited contact between the domains (Figure 5a). The average diameter of the domains was close to 400 nm, with some structures as large as several microns across. The exclusion of the larger domains resulted in the calculated mean diameter of 300 nm, accurately representing the overall size of the domains. This surface morphology suggested the spontaneous long-range ordering of the molecules at the air-water interface. The circular domains appeared to be two-dimensional micelles with total thickness 2.5–3 nm as determined by AFM that was close to ellipsometry measurements which was indicative of pancakelike organization within the monolayer with PAA chains spreading thin beneath the PS domains.<sup>12</sup> The individual domains appeared very uniform with a low surface microroughness (below 0.15 nm), indicating molecularly flat domains with no indication of ordered intramonolayer structure (Figure 5b). The decrease in the thickness of the monolayer as they were transferred from the air-water interface to the air-solid interface was apparently caused by the dehydration and collapsing of the PAA chains in contact with solid substrate (see below).

Upon compressing the monolayer to 5 mN/m, the molecules maintained the two-dimensional circular micellar structure (Figure 5c). The number of circular

(24) (a) Ulman, A. *An Introduction to Ultrathin Organic Films: From Langmuir-Blodgett to Self-Assembly*; Academic Press: Boston, 1991. (b) Spratte, K.; Riegler, H. *Makromol. Chem., Macromol. Symp.* **1991**, *46*, 113.

(25) (a) Roberts, G., Ed.; *Langmuir-Blodgett Films*; Plenum Press: New York, 1990. (b) Petty, M. *Langmuir-Blodgett Films: An Introduction*; Cambridge University Press: New York, 1996.

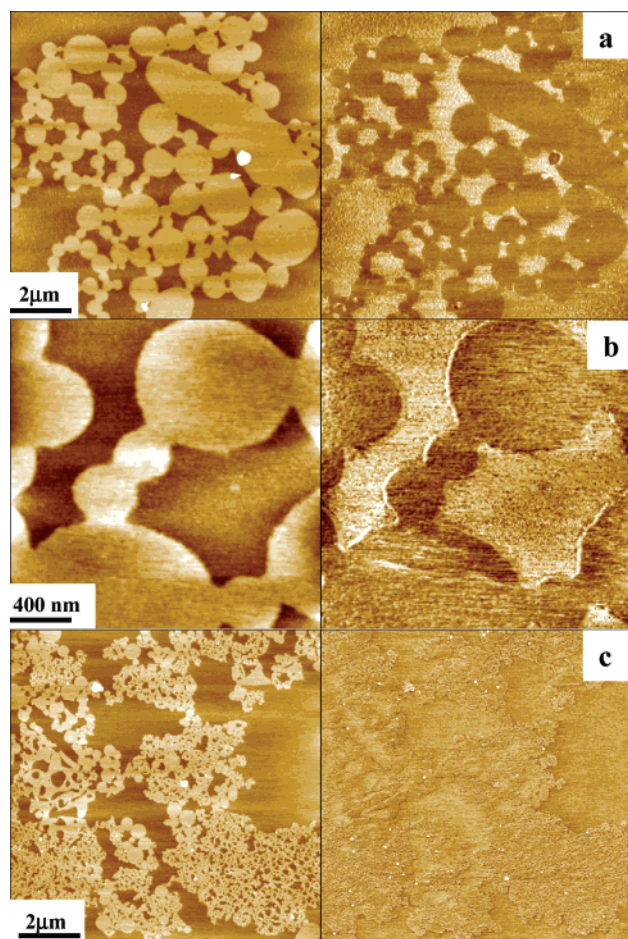


**Figure 5.** AFM images of two-dimensional micelles of  $(\text{PAA}_{30})_6\text{-s-(PS}_{40})_6$  formed (a, b) at 0 mN/m surface pressure ( $20 \text{ nm}^2$  per molecule) and (c) at low surface pressure (5 mN/m). The  $z$  range for topography (left) was 15 nm and for phase (right) was  $20^\circ$ .

domains increased as the average diameter decreased to 200 nm. The circular domains partially fused, forming larger aggregates while the surface coverage increased to nearly 50% of the total surface area that becomes close to the “jamming” limit of the random surface arrangement of circular domains.<sup>26</sup> The thickness of the PS domains remained nearly the same (2.7 nm). The further increase in the surface pressure to 10 mN/m showed additional densification of the monolayer (Figure 6a). The monolayer appeared almost uniform with small irregular defects present throughout the film indicating the circular domains merged into larger pancakelike monolayers with only a slightly higher thickness (3.1 nm). This value was still several times smaller than the maximum possible length of PS and PAA arms in their fully extended conformations and indicates their collapsed and spread state.

Upon further increase in the surface pressure to 30 mN/m the circular domains merged into a virtually continuous monolayer (Figure 6b). The reduction in the average diameter of the circular structures was offset by increasing in their number. The two-dimensional micelles formed a weblike continuous morphology similar to the larger aggregates composed of partially fused circular domains seen in Figure 6c. The coverage area of the substrate was calculated to be higher than 80% in most locations that exceeded the limits for dense surface packing of circular domains and indicated their merging with the

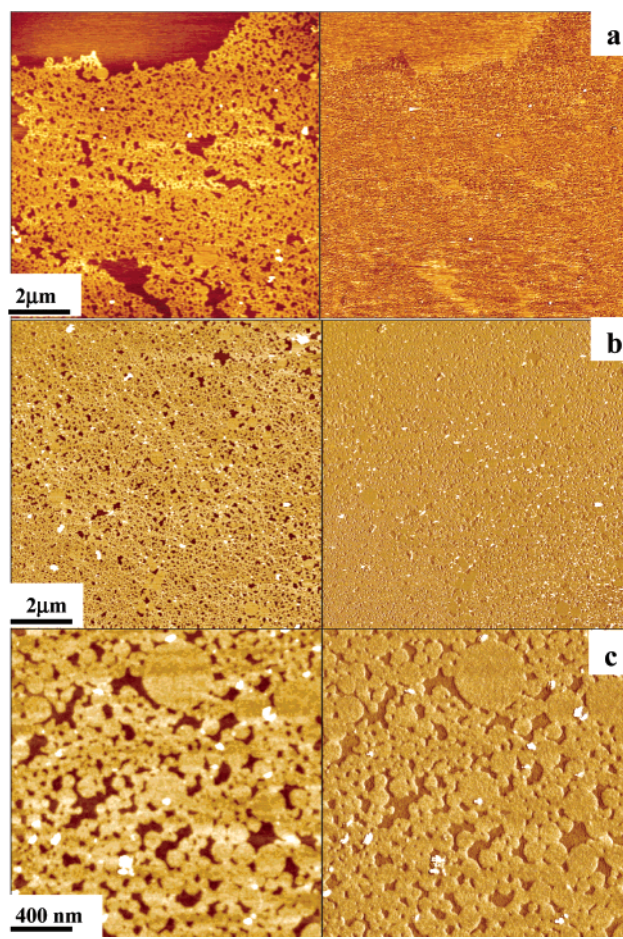


**Figure 6.** AFM images of two-dimensional micelles of  $(\text{PAA}_{30})_6\text{-s-(PS}_{40})_6$  formed at (a) moderate surface pressure (10 mN/m) and (b, c) high surface pressure (30 mN/m). The  $z$  range for topography (left) was 10 nm and phase (right) was  $10^\circ$ .

formation of uniform monolayer. The height of the domains determined from AFM cross sections increased to 3.5–4.0 nm while the overall effective thickness obtained from ellipsometry increased to nearly 5 nm, indicating a presence of a thin underlying layer below the two-dimensional micelles. An explanation for this appearance of an underlying layer was determined to be flattened molecules spread between and under the circular micelles. This structural feature may be responsible for the fact that the observed surface micelles possessed an exceedingly high two-dimensionality with diameter being nearly 100 times greater than their thickness. It was interesting to note that such circular micelles represent 2D microstructures with facial amphiphilicity (hydrophobic top and hydrophilic bottom). This was in contrast to much smaller surface micelles usually formed by linear diblocks.<sup>7</sup>

Finally, the smaller symmetric star polymer  $(\text{PAA}_{25})_6\text{-s-(PS}_{25})_6$  formed incomplete, defective domains with no indication of the circular two-dimensional micelles seen for the larger molecule (Figure 7a). At moderate pressure (10 mN/m) the molecules formed large domains up to several microns in diameter with small, rounded holes of varying size distributed throughout the surface (Figure 7a). The measured effective thickness of the monolayer was 2.6 nm, and the domain height was 2.3 nm. As the surface pressure was increased to 30 mN/m, the surface coverage increased with the effective thickness increasing to 3.7 nm. The domains formed a dense morphology with a high concentration of cracklike defects running across micron-sized surface areas (Figure 7b).

(26) Karim, A.; Tsukruk, V. V.; Douglas, J. F.; Satija, S. K.; Fetters, L. J.; Reneker, D. H.; Foster, M. D. *J. Phys. II* **1995**, *5*, 1441.

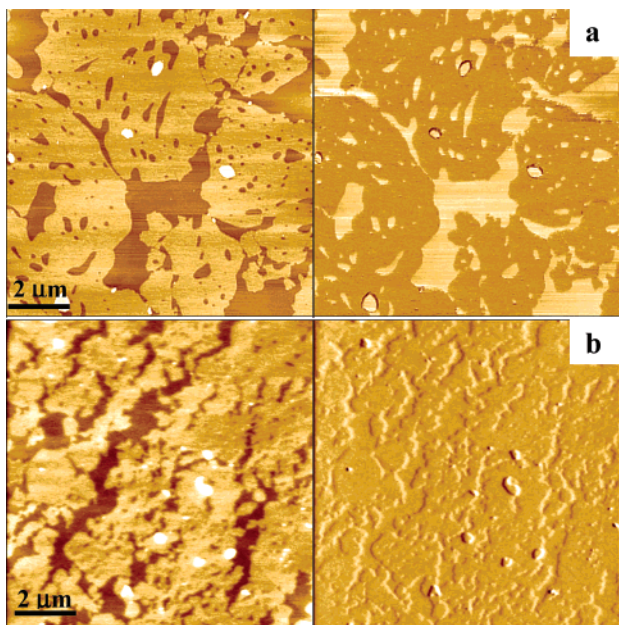


**Figure 7.** AFM images of two-dimensional micelles of  $(\text{PAA}_{25})_6\text{-s-(PS}_{25})_6$  formed at (a) moderate surface pressure (10 mN/m) and (b) high surface pressure (30 mN/m). The  $z$  range for the topography image (left) was 10 nm and the phase (right) was  $10^\circ$ .

### General Discussion

Here, we will discuss mainly the results related to asymmetric, long chain  $(\text{PAA}_{30})_6\text{-s-(PS}_{40})_6$  star polymer because of the insufficient quality of the data for star molecule with shorter chains. It seems that the decrease of the length of the PAA and PS arms in  $(\text{PAA}_{25})_6\text{-s-(PS}_{25})_6$  greatly influenced the interfacial behavior of the star block copolymer, making its monolayer structure much less defined. Significant decrease in the PS block content and the length of the both types of chains reduced segregation level, thereby disrupting the formation of the two-dimensional circular micelles.

Comparison of the monolayers parameters measured by ellipsometry, contact angle, AFM, and X-ray reflectivity allows for general conclusions to be made on structural reorganization of the monolayer in different physical states (Figure 8). In fact, this combination of experimental techniques brings to discussion very different but closely related parameters of the monolayer morphology: overall effective thickness of the monolayer at the air–water interface (X-ray reflectivity) and solid surface (ellipsometry), the separate thicknesses of top PS domains and bottom PAA phase at both water (X-ray reflectivity) and solid (AFM in combination with ellipsometry) surfaces, and the surface coverage with PS domains on the solid surface along with the presence of the hydrophobic PS chains (AFM and contact angle). The trends observed for all these parameters are very instructive and allow to make nontrivial conclusions about surface microstructure. The results discussed here are very consistent considering that they were obtained with four independent techniques on two independent sets of samples at different surfaces.

The analysis of this trend shows a consistent and sharp increase in the effective monolayer thickness at both water and solid surfaces at very low surface pressure below 5 mN/m (Figure 8). For surface pressures higher than 5 mN/m virtually constant thickness is observed. Considering significant increase in surface coverage in this range, we can attribute most of the increase observed to the formation of denser population of the domains with

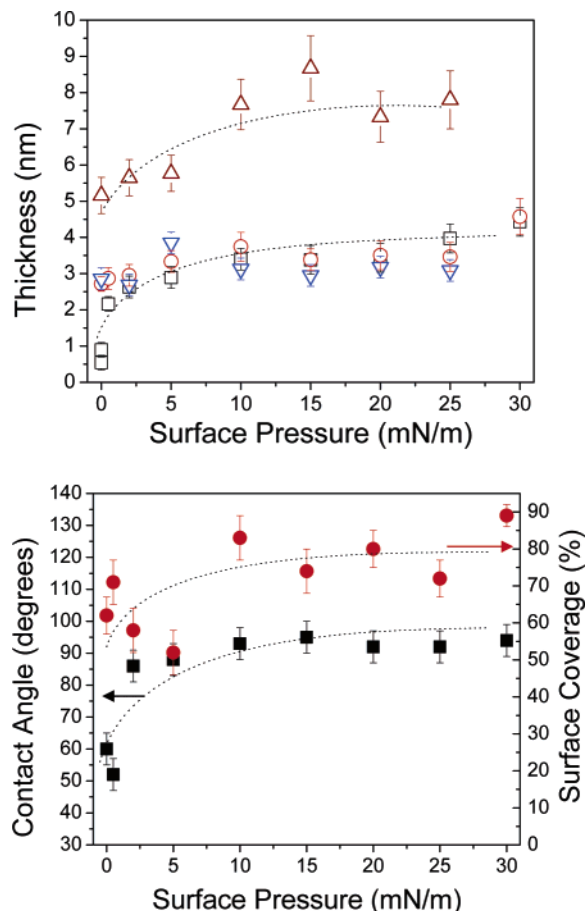


**Figure 8.** Monolayer parameters determined by X-ray reflectivity, ellipsometry, contact angle, and AFM. Top: triangles, the total monolayer thickness at air–water interface; squares, the total monolayer thickness at solid surface; circles, PS domain thickness at solid surface; inverse triangles, PS domain thickness at the air–water interface. Bottom: squares, contact angles; circles, surface coverage.

virtually unchanged thickness (except very low surface areas for pressures below 2 mN/m). This conclusion is also supported by isotherm data which shows that the surface area per molecule at surface pressures of 5 mN/m and higher is very close to  $A_0$ , which is mainly defined by the rigid cores as we discussed above (Figure 2). The contact angle initially increases sharply to  $95^\circ$  and stays constant in a whole range of pressures (Figure 8). This value is identical to that observed for grafted PS chains in solid state<sup>27</sup> and indicates uniform composition of the monolayer surface composed of PS chains.

However, the thickness of the condensed monolayer at the water surface and on the solid substrate differs more than twice:  $7.9 \pm 0.5$  nm vs  $3.1 \pm 0.5$  nm (Figure 8). The much smaller total thickness for solid-supported LB monolayers as compared with the same monolayer at the air–water interface indicates significant difference in internal microstructure of the monolayers. Direct comparison of the total thickness of the monolayer and the thickness of the PS phase immediately allows concluding that the PAA chains submerged in water are extended to  $4.8 \pm 0.6$  nm but are spread in the thin layer of around 0.3 nm at the solid surface. Constant extension of the PAA chains over almost a whole region of surface pressure tested (from 5 to 30 mN/m) can be attributed to the factor of limited grafting density imposed by the presence of the

(27) Luzinov, I.; Julthongpipit, D.; Tsukruk, V. V. *Macromolecules* **2000**, *33*, 7629.

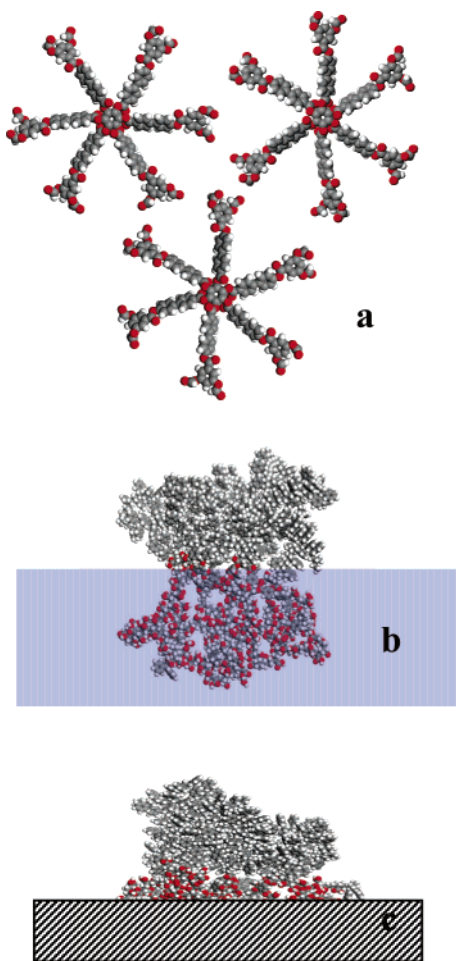


**Figure 9.** Schematic of  $(\text{PAA}_{30})_6\text{-s-(PS}_{40})_6$  monolayer microstructure: (a) top view of the core to core packing behavior (the polymeric arms are removed for clarity), side view of the molecule packing at the air–water interface (b), and the air–solid interface (c).

sizable rigid cores which prevent the truly brush regime and full extension of the PAA chains. This is in a sharp contrast with conventional block copolymers with pointlike junctions where the molecules undergo constant change under compression.<sup>7,28</sup>

The height of the PS domain determined by AFM was consistent with the thickness of the PS blocks determined by X-ray reflectivity as well as ellipsometry at all surface pressures (Figure 8). Unlike PAA chains which undergo tremendous spreading in the course of transfer to a solid surface, the thickness of PS domains remains almost unchanged, around 3 nm. This last value is fairly close to the dimensions of the collapsed PS chains (Table 1). Thus, despite the significant surface area available for random coiled PS chains provided by the large rigid core, even higher compression does not affect the state of the PS chains.

Finally, Figure 9 provides a schematic representation of the segregation behavior of the star molecules  $(\text{PAA}_{30})_6\text{-s-(PS}_{40})_6$  as revealed by this study. At the air–water interface, the PAA arms submerge into the water subphase, creating a dense, hydrated PAA layer below the core plane with significantly extended PAA chains in the condensed monolayer state. To form a more stable micellar structure, the PS chains aggregate above the aromatic core, creating a collapsed PS layer. Upon transfer to the solid substrate, the PAA chains dehydrate and spread very thin between hydrophobic PS layer and hydrophilic silicon substrate (Figure 9). The moderate length of the PS and PAA chains allows the chains to form dense layers, occupying the space directly above and below the aromatic core. This is also responsible for the formation of stable circular micellar structures with diameter of 200–300 nm which include several thousand molecules and are distinguished two-dimensional structures with “two faces”: highly hydrophobic and highly hydrophilic. Remarkable stable molecular packing of the star molecules with virtually unchanged characteristics in a wide range of compressions is a signature of the amphiphilic star polymer with rigid core studied here. We suggest that this is caused by limited grafting density of the PS and PAA chains attached to the sizable rigid core which prevents the monolayer to undergo reorganization from “gaseous” to condensed state. These changes triggered by decreasing surface area per molecule usually result in a wide variety of dot, spaghetti-like, rectangular, or lamellar surface morphologies observed in linear or modestly branched amphiphilic diblock copolymers of different types.<sup>12,28–31</sup> Stability of these micellar structures at the water and solid surfaces over a wide range of surface pressures is a signature of these amphiphilic star polymers, making them unique polymeric surfactants.

**Acknowledgment.** The authors thank J. Holzmüller, M. Ornatska, and S. Peleshanko for technical assistance during experiments. Funding from the National Science Foundation, DMR-0308982 and Imperial Chemical Industries, SRF 2112, is gratefully acknowledged. The Midwest Universities Collaborative Access Team (MUCAT) sector at the APS, where X-ray studies were conducted, is supported by the U.S. Department of Energy, Basic Energy Sciences, Office of Science, through the Ames Laboratory under Contract W-7405-Eng-82. Use of the APS was supported by the U.S. Department of Energy, Basic Energy Services, Office of Science, under Contract W-31-109-Eng-38.

LA048548X

(28) Tsukruk, V. V.; Genson, K.; Peleshanko, S.; Markutsya, S.; Lee, M.; Yoo, Y.-S. *Langmuir* **2003**, *19*, 495.

(29) Williams, D. R.; Fredrickson, G. H. *Macromolecules* **1992**, *25*, 3561.

(30) Li, W.; Gersappe, D. *Macromolecules* **2001**, *34*, 6783.

(31) Peleshanko, S.; Jeong, J.; Gunawidjaja, R.; Tsukruk, V. V. *Macromolecules* **2004**, *37*, 6511.